american physiological society

JNP JOURNAL OF NEUROPHYSIOLOGY

J Neurophysiol 128: 1307–1311, 2022.
First published October 19, 2022; doi:10.1152/jn.00402.2022

RAPID REPORT

Heritability of brain neurovascular coupling

Peka Christova,[1,2] Kâmil Uğurbil,[2,3] and Apostolos P. Georgopoulos[1,2]

[1]*Department of Veterans Affairs Health Care System, The Functional Neuroimaging Research Group, Brain Sciences Center, Minneapolis, Minnesota;* [2]*Department of Neuroscience, University of Minnesota Medical School, Minneapolis, Minnesota; and* [3]*Center for Magnetic Resonance Research, Department of Radiology, University of Minnesota Medical School, Minneapolis, Minnesota*

Abstract

The moment-to-moment variation of neurovascular coupling in the brain was determined by computing the moment-to-moment turnover of the blood-oxygen-level-dependent signal (TBOLD) at resting state. Here we show that *1*) TBOLD is heritable, *2*) its heritability estimates are highly correlated between left and right hemispheres, and *3*) the degree of its heritability is determined, in part, by the anatomical proximity of the brain areas involved. We also show that the regional distribution of TBOLD in the cortex is significantly associated with that of the vesicular acetylcholine transporter. These findings establish that TBOLD as a key heritable measure of local cortical brain function captured by neurovascular coupling.

NEW & NOTEWORTHY Here we show that the sample-to-sample turnover of the resting state fMRI blood-oxygen-level-dependent turnover (TBOLD) is heritable, the left and right hemisphere TBOLD heritabilities are highly correlated, and TBOLD heritability varies among cortical areas. Moreover, we documented that TBOLD is associated with the regional cortical distribution of the vesicular acetylcholine transporter.

blood oxygen level dependent turnover; TBOLD; fMRI; heritability; resting-state functional MRI

INTRODUCTION

The blood-oxygen-level-dependent (BOLD) signal is the most commonly used measure in brain functional magnetic resonance imaging (fMRI). Under conditions of stimulation or task performance, it reflects the hemodynamic response to local synaptic activity (1) mediated by neurovascular coupling (NVC), a complex phenomenon involving diverse cellular and chemical components (2, 3). In the resting state, when neural activity is more or less constant, neural events seem to contribute significantly but relatively little (up to 10%) to the BOLD signal (4). Therefore, it is reasonable to suppose that the moment-to-moment change in the BOLD signal (i.e., its turnover, TBOLD) reflects predominantly neurovascular events, including involvement of the glia (5), and can thus serve as an index of NVC sensitivity in a given brain area, ranging substantially across areas (6). Given the hard-wired morphological and functional arrangements among neurons, glia, neurotransmitters, neuromodulators, etc., in the neurovascular unit (3), we sought to determine whether TBOLD is heritable and, if so, the possible association of the degree of heritability of two brain areas with the proximity of their anatomical location in the brain. For that purpose, we computed Falconer's heritability h^2 (7) of mean TBOLD (mTBOLD) for 35 areas of the cerebral cortex using data from a total of 406 genetically confirmed participants in the healthy young adults database of the Human Connectome Project (HCP) (www.humanconnectome.org). We used Falconer's original formula (7) based on intraclass correlations because of its simplicity and broad sense heritability estimate (8).

MATERIALS AND METHODS

Participants

Data were retrieved from the healthy young adults database of the Human Connectome Project (HCP) (www.humanconnectome.org), a total of genetically confirmed 203 twin pairs. There were 130 monozygotic pairs [MZ, N = 260, means (SD) years old 29.3 (3.3) with 110 males 27.9 (3.4) and 150 females 30.4 (2.8)]. There were 73 dizygotic pairs [DZ, N = 146, means (SD) years old 29.0 (3.6) with 58 males 26.6 (3.2) and 88 females 30.6 (2.8)]. There were 406 total participants.

Correspondence: A. P. Georgopoulos (omega@umn.edu).
Submitted 21 September 2022 / Accepted 13 October 2022

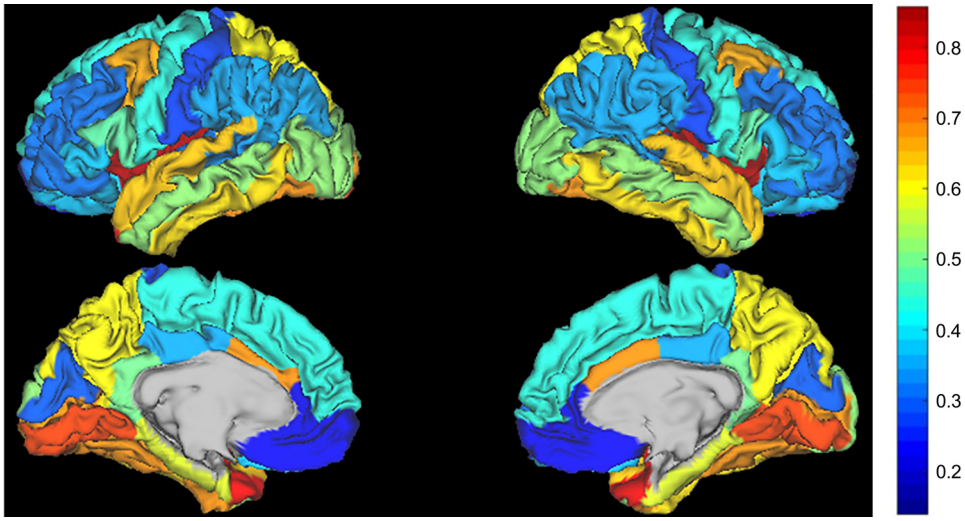

Figure 1. Color map of the regional cortical distribution of mTBOLD h^2. mTBOLD, mean TBOLD.

All participants provided written informed consent, and the Institutional Review Board of Washington University approved the research protocol. The Research and Development Committee of the Minneapolis Veterans Affairs Medical Center approved this study.

fMRI Data Collection

fMRI data were collected at Washington University (St. Louis, MO) using a customized Siemens 3 T scanner with a standard 32-channel receiver head coil. The structural scans included T1-weighted and T2-weighted images, acquired at a high resolution of 0.7 mm (9). Resting-state fMRI (rfMRI) images were collected using a gradient-echo echo planar imaging (EPI) sequence with the following parameters: repetition time (TR) = 720 ms, echo time (TE) = 33.1 ms, flip angle = 52 degrees, field of view (FOV) = 208 × 180 mm (RO × PE), matrix = 104 × 90 (RO × PE), 2.0 mm isotropic voxels, 72 axial slices, and multiband factor = 8. The HCP's minimally preprocessed pipeline removes spatial distortions, realigns volumes to compensate for subject motion, registers the fMRI data to the structural MRI, and transforms to the standard Montreal Neurological Institute (MNI) space (9).

rfMRI Time Series Extraction and Processing

For each subject, there were 1200 blood oxygenation level-dependent (BOLD) values per vertex with different numbers of vertices in the area, depending on the size of the area. The BOLD time series were extracted from rfMRI data using MATLAB (R2016b, MathWorks, Natick, MA). For each participant verities of the whole brain were grouped into different areas based on the Desikan–Killiany atlas (10) parcellation scheme. The cortical sulci and gyri of the brain are labeled in 70 areas (35 in the left and 35 in the right hemisphere). These automatically labeled areas for each participant are as follows: banks of the superior temporal sulcus, caudal anterior cingulate gyrus, caudal middle frontal gyrus, cuneus, entorhinal gyrus, frontal pole, fusiform gyrus, hippocampus, inferior frontal gyrus pars opercularis, inferior frontal gyrus pars orbitalis, inferior frontal gyrus pars triangularis, inferior parietal lobule, inferior temporal gyrus, insula, isthmus of cingulate gyrus, lateral occipital gyrus, lateral orbitofrontal gyrus, lingual gyrus, medial orbitofrontal gyrus, middle temporal gyrus, paracentral gyrus, parahippocampal gyrus, pericalcarine gyrus, postcentral gyrus, posterior cingulate gyrus, precentral gyrus, precuneus,

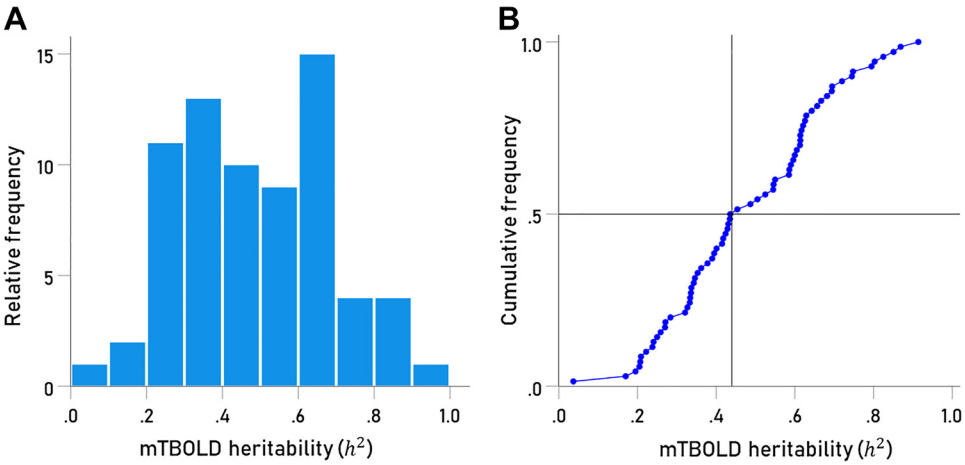

Figure 2. Relative frequency distribution (*A*) and cumulative frequency distribution (*B*) of mTBOLD h^2. N = 70 areas. mTBOLD, mean TBOLD.

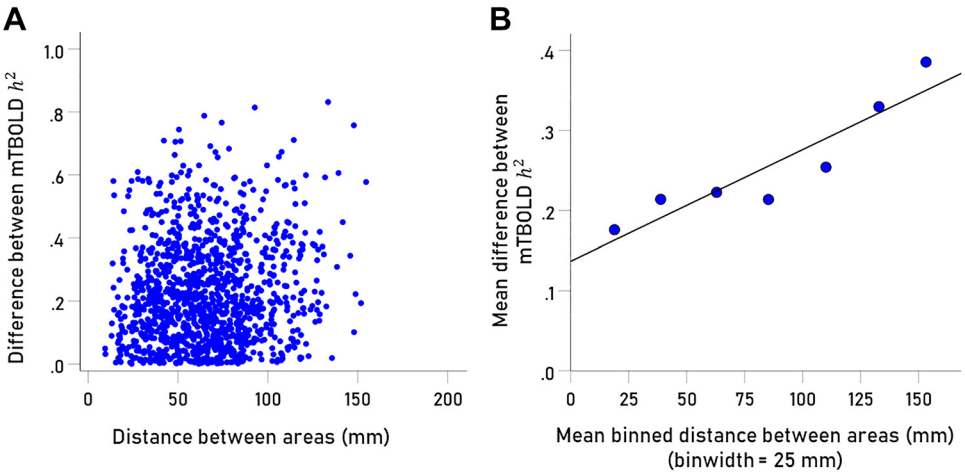

Figure 3. *A*: scatter plot of difference between mTBOLD h^2 and distance between corresponding areas; r = 0.113, P = 0.00 0099, N = 1,190. *B*: the average difference in mTBOLD h^2 is plotted against the average distance of the corresponding areas, averaged over 25 mm distance bins; r = 0.921, P = 0.003. See text for details. mTBOLD, mean TBOLD.

rostral anterior cingulate gyrus, rostral middle frontal gyrus, superior frontal gyrus, superior parietal lobule, superior temporal gyrus, supramarginal gyrus, temporal pole, and transverse temporal gyrus. Finally, for each participant and each area, the mean values of x y z coordinates of the vertices were found and averaged across participants to obtain mean x y z area coordinates.

Data Preprocessing

A robust, nonparametric estimate of BOLD turnover was obtained in three steps described in detail in James et al. (6). Briefly, *1*) single BOLD time series for a given k^{th} vertex were first-order differenced by applying an Auto Regressive Moving Average (ARIMA) model of (0,1,0) (11) using MATLAB (version R2016b); *2*) the median of the absolute values of the differenced time series was computed; and *3*) this median value was divided by 0.72 s to yield the BOLD turnover per second (TBOLD), since TR = 0.72 s:

$$\text{TBOLD}^k = \text{median of absolute value of BOLD change}/0.72. \quad (1)$$

Finally, the mean TBOLD for each ROI (across M vertices in the ROI) was computed and used for further analyses:

$$\text{mTBOLD} = \frac{1}{M}\sum_{k}^{k=1,M} \text{TBOLD}^k. \quad (2)$$

Intraclass Correlations and Heritability

The intraclass correlation coefficient (ICC) of mTBOLD was calculated for each ROI for MZ and DZ twin pairs, and the genetic heritability of mTBOLD was determined using Falconer's formula (7):

$$h^2 = 2(\text{ICC}_{\text{MZ}} - \text{ICC}_{\text{DZ}}). \quad (3)$$

Proximities in Heritability and Anatomical Location of Corresponding Areas

Let h^2_k, h^2_m be the heritabilities for areas k and m, respectively; and let $(x_k y_k z_k)$ and $(x_m y_m z_m)$ be the mean x, y, z coordinates of those areas. We took the absolute difference in heritabilities as a measure of proximity of heritabilities:

$$\text{d}h^2_{k,m} = h^2_k - h^2_m. \quad (4)$$

The Euclidean distance between the mean (x y z) coordinates of the anatomical location of the corresponding areas was used as an estimate of their anatomical proximity:

$$\text{d}\,location_{k,m} = \sqrt{(x_k - x_m)^2 + (y_k - y_m)^2 + (z_k - z_m)^2}. \quad (5)$$

This measure was computed separately within the left and right hemispheres. The N for these measures was 1,190 pairs, given 35 areas, hence $\frac{35\times34}{2}$ = 595 pairs, per hemisphere.

Regional Distribution of Vesicular Acetylcholine Transporter in the Human Brain

We compared the regional distribution of mTBOLD to that of the strength of binding of vesicular acetylcholine transporter (VAChT) in the normal human brain (12), as follows. Table 1 of Albin et al. (12) gives estimates of VAChT binding in various brain areas, with a Brodmann's area (BA) identification for cortical areas. We assigned the corresponding BA number to each one of the 35 cortical areas we analyzed; VAChT binding estimates were available in Table 1 of Albin et al. (12) for 30 of our 35 areas; VAChT values were not given

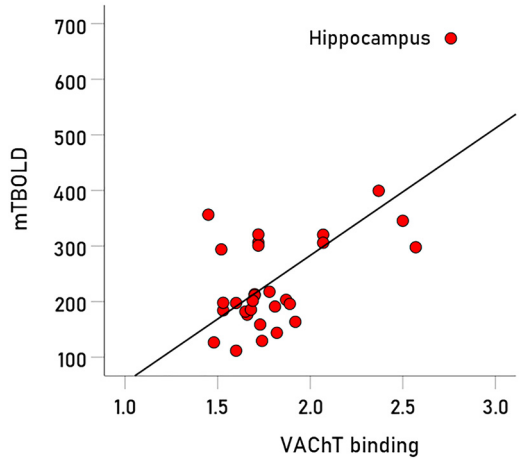

Figure 4. Scatter plot of mTBOLD against estimates of VAChT. r = 0.675, P = 0.000043, N = 30. See text for details. mTBOLD, mean TBOLD; VAChT, vesicular acetylcholine transporter.

for BA37 (fusiform gyrus), BA38 (temporal pole), BA40 (supramarginal gyrus), BA41 (banks of superior temporal sulcus), BA42 (transverse temporal gyrus). Therefore, correlations were computed between TBOLD (averaged between left and right hemispheric values) and VAChT binding (also averaged the same way) for the remaining 30 areas.

Statistical Analyses

Linear regression and Pearson correlation were used to evaluate the association between $dh^2_{k,m}$ and $dlocation_{k,m}$, separately within each hemisphere. Multiple linear regression was used to assess the possible dependence of h^2 on mean (x y z) coordinates. Analyses were conducted using MATLAB (v. R2016b), Intel Fortran Compiler (v. 2021.2.0, extension v. 19.2.0061.16), and IBM-SPSS (v. 27).

RESULTS AND DISCUSSION

We found substantial mTBOLD heritabilities (Fig. 1). The relative and cumulative frequencies of the heritability estimates of mTBOLD are shown in Fig. 2*A* and *B*, respectively. Heritabilities of mTBOLD ranged among areas, from 0.914 for the right insula to 0.037 for the left frontal pole. The means (± SE) mTBOLD heritability was 0.483 ± 0.024 (N = 2 hemispheres × 35 areas/hemisphere = 70 areas total), with 45% of heritabilities exceeding 0.5. Heritabilities of mTBOLD were significantly correlated between the two hemispheres (r = 0.657, P = 0.00018, N = 35). A multiple linear regression of mTBOLD h^2 against the (x y z) coordinates of the corresponding areas revealed a significant, linear increase of mTBOLD h^2 along the y-axis, from anterior to posterior (P = 0.003). A similar increase of mTBOLD h^2 was found along the z-axis, from superior to inferior but did not reach statistical significance (P = 0.057); there was no significant variation of mTBOLD h^2 along the medio-lateral x-axis (P = 0.937). This association of mTBOLD h^2 with the anatomical location was further evaluated by assessing the correlation between the difference in mTBOLD h^2 of two areas and the distance in their mean (x y z) coordinates. Indeed, we found a small but highly statistically significant positive correlation between these two measures (r = 0.113, P = 0.000099, N = 1,190 pairs). All data are plotted in Fig. 3*A*, and mean mTBOLD h^2 for binned between-area distances in Fig. 3*B*.

These findings document the heritability of TBOLD, its variation across brain areas, its significant correlation between hemispheres, and its orderly association with cortical anatomy. TBOLD in the resting state reflects local hyperemia modulated by acetylcholine (2, 3, 13), a known brain vasodilator (14, 15). Indeed, we found a significant positive association between the regional cortical distributions of mTBOLD and the vesicular acetylcholine transporter (VAChT) (14) (Fig. 4), confirming previous findings in a different group of participants (6).

Given that resting state, TBOLD reflects mostly neurovascular events (4), which are very complex (2, 3), it would be difficult to attribute its heritability to the combined heritabilities of individual components of the neurovascular unit. A more parsimonious hypothesis is to attribute TBOLD heritability to a factor with which TBOLD is associated as a whole, namely, the distribution of acetylcholine projections in the cortex. Genetic heritability studies of VAChT would help test this hypothesis.

DATA AND MATERIALS AVAILABILITY

Data are publicly available from the websites mentioned in the MATERIALS AND METHODS. Data were provided by the Human Connectome Project, WU-Minn Consortium (Principal Investigators: David Van Essen and Kâmil Uğurbil; 1U54MH091657) funded by the 16 National Institutes of Health (NIH) institutes and centers that support the NIH Blueprint for Neuroscience Research; and by the McDonnell Center for Systems Neuroscience at Washington University.

GRANTS

Partial funding for this study was provided by the McKnight Presidential Chair of Cognitive Neuroscience, the American Legion Brain Sciences Chair), and the U.S. Department of Veterans Affairs.

DISCLAIMERS

The sponsors had no role in the current study design, analysis or interpretation, or in the writing of this paper. The contents do not represent the views of the U.S. Department of Veterans Affairs or the United States Government.

DISCLOSURES

No conflicts of interest, financial or otherwise, are declared by the authors.

AUTHOR CONTRIBUTIONS

A.P.G. conceived and designed research; P.C. and A.P.G. analyzed data; P.C., K.U., and A.P.G. interpreted results of experiments; P.C. and A.P.G. prepared figures; P.C. and A.P.G. drafted manuscript; P.C., K.U., and A.P.G. edited and revised manuscript; P.C., K.U., and A.P.G. approved final version of manuscript.

REFERENCES

1. **Logothetis NK**, **Pauls J**, **Augath M**, **Trinath T**, **Oeltermann A.** Neurophysiological investigation of the basis of the fMRI signal. *Nature* 412: 150–157, 2001. doi:10.1038/35084005.
2. **Hillman EMC.** Coupling mechanism and significance of the BOLD signal: a status report. *Annu Rev Neurosci* 37: 161–181, 2014. doi:10.1146/annurev-neuro-071013-014111.
3. **Iadecola C.** The neurovascular unit coming of age: a journey through neurovascular coupling in health and disease. *Neuron* 96: 17–42, 2017. doi:10.1016/j.neuron.2017.07.030.
4. **Lu H**, **Jaime S**, **Yang Y.** Origins of the resting-state functional MRI signal: potential limitations of the "neurocentric" model. *Front Neurosci* 13: 1136, 2019. doi:10.3389/fnins.2019.01136.
5. **Iadecola C**, **Nedergaard M.** Glial regulation of the cerebral microvasculature. *Nat Neurosci* 10: 1369–1376, 2007. doi:10.1038/nn2003.
6. **James LM**, **Christova P**, **Georgopoulos AP.** BOLD turnover in task-free state: variation among brain areas and effects of age and human leukocyte antigen (HLA) DRB1*13. *Exp Brain Res* 240: 1967–1977, 2022. doi:10.1007/s00221-022-06382-y.
7. **Falconer DS.** The inheritance of liability to certain diseases, estimated from the incidence among relatives. *Ann Human Genet* 29: 51–76, 1965. doi:10.1111/j.1469-1809.1965.tb00500.x.
8. **Mayhew AJ**, **Meyre D.** Assessing the heritability of complex traits in humans: methodological challenges and opportunities. *Curr Genomics* 18: 332–340, 2017. doi:10.2174/1389202918666170307161450.
9. **Glasser MF**, **Sotiropoulos SN**, **Wilson JA**, **Coalson TS**, **Fischl B**, **Andersson JL**, **Xu J**, **Jbabdi S**, **Webster M**, **Polimeni JR**, **Van Essen**

DC, **Jenkinson M**; **WU-Minn HCP Consortium.** The minimal preprocessing pipelines for the Human Connectome Project. *NeuroImage* 80: 105–124, 2013. doi:10.1016/j.neuroimage.2013.04.127.

10. **Desikan RS**, **Ségonne F**, **Fischl B**, **Quinn BT**, **Dickerson BC**, **Blacker D**, **Buckner RL**, **Dale AM**, **Maguire RP**, **Hyman BT**, **Albert MS**, **Killiany RJ.** An automated labeling system for subdividing the human cerebral cortex on MRI scans into gyral based regions of interest. *NeuroImage* 31: 968–980, 2006. doi:10.1016/j.neuroimage.2006.01.021.
11. **Box GE**, **Jenkins JM.** *Time Series Analysis: Forecasting and Control* (2nd ed.). San Francisco, CA: Holden-Day, 1976.
12. **Albin RL**, **Bohnen NI**, **Muller MLTM**, **Dauer WT**, **Sarter M**, **Frey KA**, **Koeppe RA.** Regional vesicular acetylcholine transporter distribution in human brain: A [^{18}F]fluoroethoxybenzovesamicol positron emission tomography study. *J Comp Neurol* 526: 2884–2897, 2018. doi:10.1002/cne.24541.
13. **Zaldivar D**, **Rauch A**, **Logothetis NK**, **Goense J.** Two distinct profiles of fMRI and neurophysiological activity elicited by acetylcholine in visual cortex. *Proc Natl Acad Sci USA* 115: E12073–E12082, 2018. doi:10.1073/pnas.1808507115.
14. **Heistad DD**, **Marcus ML**, **Said SI**, **Gross PM.** Effect of acetylcholine and vasoactive intestinal peptide on cerebral blood flow. *Am J Physiol Heart Circ Physiol* 239: H73–H80, 1980. doi:10.1152/ajpheart.1980.239.1.H73.
15. **Scremin OU**, **Jenden DJ.** Cholinergic control of cerebral blood flow in stroke, trauma and aging. *Life Sci* 58: 2011–2018, 1996. doi:10.1016/0024-3205(96)00192-0.